Egypt. J. Chem. **Vol. 63.** No. 10. pp. 3735 - 3745 (2020)

Egyptian Journal of Chemistry

http://ejchem.journals.ekb.eg/

Oxidation Behavior of Porous Ni- 4 and 8 wt %Cr Alloys in Air at 1273K

Lamiaa Z. Mohamed,[a,*] Wafaa A. Ghanem,[b] Omayma A. El kady,[c]

Mohamed. M. Lotfy,[a] Hafiz A. Ahmed,[a] Fawzi A. Elrefaie,[a]

[a]*Mining, Petroleum and Metallurgical Engineering Dept., Faculty of Engineering, Cairo University, Giza, 12613, Egypt*

[b]*Corrosion and Surface Protection, Central Metallurgical Research and Development Institute (CMRDI), Helwan, Egypt*

[c]Powder Technology Division, Central Metallurgical Research and Development Institute (CMRDI), Helwan, Egypt

Abstract

Oxidation behavior of porous Ni-4 and 8 wt% Cr pellets prepared by conventional powder metallurgy was investigated. The pellets were oxidized in air at 1273K for 100 h. The oxidation kinetics were measured by using gravimetric method. The oxide layer morphology and, the surfaces topography and the cross-section microstructure of the oxidized pellets were investigated using X-ray diffraction, optical microscopy, scanning electron microscopy and X-ray energy dispersive analysis. The oxidation rate was initially rapid and then gradually decreased until realizing a constant rate after oxidation time of about 40 h for the 4 wt %Cr pellets with linear rate constant of about $8x10^{-8}$ (g/cm^2)/sec. For the 8 wt %Cr pellets, the linear rate constant was about $20x10^{-8}$ (g/cm^2).sec which was achieved after 72 h. Porous nickel oxide scales were formed on the 4 and 8 wt %Cr substrates. Finally, the growth of the oxide scale was explained on the basis of inward migration of molecular oxygen through the porous oxide scale; accordingly, the newly oxide atomic layers were added at the scale/metal interface.

Keywords: Porous Ni-4 and 8 wt%Cr alloys; High temperature oxidation; Inward molecular oxygen migration; Linear kinetics; Porous oxide scale microstructure

1. Introduction

The oxidation of Ni and Ni–Cr alloys, which are of technological importance in many industrial applications [1], is of scientific interest as a model alloy system to understand the doping effect on oxidation kinetics and the passivation mechanisms at high temperature [2]. For example, the boiler tubes degrades at high temperatures due to the erosion as well as corrosion [3, 4]. Traditional oxidation studies usually focus on steady state oxidation where all oxide phases might be developed to form the thermodynamically stable oxide scale. Kinetic studies and examination of the microstructure are insufficient to understand the oxidation mechanisms. For example, adding a small amount (<8%) of chromium to nickel increases the oxidation rate rather than passivating the alloy; this behavior is attributed not only to increasing the number of cation vacancies in the $Ni_{1-x}O$ p-type oxide due to the doping effect of Cr^{+3} in the cationic lattice of nickel oxide but also might be due to increasing the easy diffusion paths (e.g. grain boundaries and cavities) in the oxide scale. Therefore, studies of the early stages and dynamic processes of alloy oxidation are critical to understand the controlling mechanisms [2].

For alloys of greater than 2 at% Cr, a complex exchange of chromium among the three oxide phases NiO doped with Cr, the spinel, $NiCr_2O_4$, and Cr_2O_3 has been detected. This chromium exchange was reflected on the rate of

*Corresponding author e-mail: lamiaa.zaky@cu.edu.eg ; (Lamiaa Zaky Mohamed).
Receive Date: 11 October 2019, Revise Date: 13 February 2020, Accept Date: 01 March 2020
DOI: 10.21608/EJCHEM.2020.18068.2100

increase of oxidation rate with chromium addition to the alloy [5, 6]. Wagner and Zimens obtained oxidation data for Ni-Cr alloys at 1237 K. The dependence of the oxidation rate on the chromium atomic percent obtained by the mentioned investigators showed the expected increase in oxidation rate with chromium addition up to roughly 10 at% Cr [5]. A linear dependence of the oxidation rate on the chromium content between 0.36 and 8.6 at% Cr is observed. A definite slope change is indicated at about 2 at% Cr. The maximum oxidation rate was detected at about 8.6 at% Cr [5].

The cold rolled material yielded oxidation rates which were substantially higher than the rates of the corresponding large grained material [7]. Therefore, introducing internal stresses into the matrix of the metal substrates before oxidation might increase the oxidation rate. These data indicate a maximum oxidation rate at roughly 6 at% Cr [5]. The separation of the outside layer of large NiO crystals from the interior zone was very noticeable for the 9.5 at% oxide. It proved, in fact, to be quite difficult to obtain a full section of this oxide. In view of the X-ray analysis, the region of fine structure must be associated with the Cr_2O_3 and spinel phases [5]. There is evidence for chromium-rich second phase particles in or beneath the NiO for alloys containing as little as l.8%Cr and 4.7%Cr. However, it appears that chromium solubility in NiO may be raised considerably with extended exposure, which would increase this limiting concentration level for solubility. A further point worth noting is that accepted transport mechanisms in NiO itself have also been questioned recently [8]. It may also be proposed that second-phase particles and even Cr^{3+} ions in the NiO lattice affect the plasticity, strength and adhesion of the scale, tending to promote cracking and porosity. In addition, the enhancement of growth rate due to Cr^{3+} ions increasing the cation vacancy concentration may itself have mechanical consequences in the scale by causing greater cracking or porosity, thus promoting yet faster scaling rates. It would be interesting to know whether such behavior tends to promote double-layer scales, which have been reported for nickel and Ni-Cr alloys and, if so, how the chromium is distributed between the layers [8].

Certainly in the range Ni-5-10% Cr, the scale is complex, with an outer layer consisting of nearly pure NiO grown over two-phases inner layer of NiO and $NiCr_2O_4$ which is attached to an alloy containing Cr_2O_3 sub-scale. There are two reasonably plausible theories to explain such structures. One proposes that when the alloy is exposed to oxidizing environment, both NiO and Cr_2O_3 are formed initially but rapidly combine and coalesce to give $NiCr_2O_4$ granules in a matrix of excess NiO, so effectively forming the inner layer [8]. Partial dissociation of NiO occurs at the alloy/oxide interface and oxygen diffuses into the alloy causing preferential oxidation of Cr to Cr_2O_3 at grain boundaries and in grains of what becomes essentially pure nickel. As the external scale develops by outward diffusion of nickel, the granules become incorporated into the inner layer where they are rapidly converted to $NiCr_2O_4$. The second theory requires a porous inner layer. The outer layer grows by the outward diffusion of Ni^{2+} ions and electrons and the inner layer by the inward diffusion of oxygen gas, produced by dissociation of NiO in the voids at the interface between the two layers. Oxygen also diffuses into the bulk alloy where chromium is preferentially oxidized to Cr_2O_3 the alloy matrix then is transferred to pure nickel. There is also some Ni^{2+} diffusion out through bridges of scale in the porous inner layer [8]. The main aim of this investigation to study the high temperature behavior of porous Ni-4 and 8 wt% Cr pellets prepared by conventional powder metallurgy at 1273 K in air for 100h.

2. Experimental

The pellets of the 4 and 8 wt% Cr were fabricated from a mix of nickel and chromium powders. The nickel powder consisted of nearly spherical particles whose size is less than 149 μm. The chromium particles are irregular in shape with particle size less than 149 μm. The compositions of nickel and chromium powders as given by the suppliers are listed in Table 1. Both compositions were verified by wet chemical analysis. The results obtained by wet chemical analysis are also listed in Table 1. The data in Table 1 indicates that the total impurity level in the nickel powder is about 0.1% and that of the chromium powder is about 0.01%.

TABLE 1. The chemical analysis of nickel and chromium powders

Elements, %	Composition			
	Nickel Powder		Chromium Powder	
	Given by the supplier*	Obtained by wet chemical analysis**	Given by the supplier*	Obtained by wet chemical analysis**
C	0.08	0.07	--	--
S	0.001	N.D.	--	--
Fe	0.01	0.015	0.0003	0.001
Cd	--	--	<0.0004	N.D.
Mg	--	--	0.00004	N.D.
Ag	--	--	0.0007	0.001
Pb	--	--	0.00004	N.D.
Ni	Bal.	99.9	--	--
Cr	--	--	Bal.	99.99

* analyses given by the supplier (Dop. Company)

**wet chemical analysis in the laboratories of the "Egyptian Mineral Resources Authority (EMRA)"

Green pellets were prepared by compacting the powder mix under 420 MPa. The pellets were then sintered at 1473K for 2 h. Sintered pellets with 18.9-19.0 mm in diameter and 3.6-3.7 mm in thickness were produced. The average values of the measured apparent densities of the sintered pellets according to Eq. 1. was 6.84 and 6.67 g/cm^3 for the 4 and 8 wt% Cr pellets, respectively. Porosity values of the pellets according to Eq. 2. were estimated, in turn, to be about 22.6% and 22.9% for the 4 and 8 wt% Cr pellets, respectively.

$$\text{Densification} = (\rho_{app} / \rho_{true}) * 100 \quad (1)$$

$$\text{Porosity} = [(\rho_{true} - \rho_{app})/\rho_{true}] * 100 \quad (2)$$

where ρ_{app} is the apparent density of the alloy while ρ_{true} is the true density for the alloy.

The oxidation kinetics of three pellets of each type in air at 1273K were obtained at 100 h by detecting the change of the weight gain per unit area with time for each pellet. For first approximation, the area of open pores of each pellet was assumed to be negligible at the initial stage of oxidation with respect to the surface area of the pellet. The weight gain was carried out during the oxidation test by employing gravimetric method; a microbalance with an accuracy of 10^{-4} g was utilized in this investigation.

X-ray diffractometry (XRD) was used for identification of oxide phases formed during the oxidation process; "X'Pert PRO PAN Analytical Diffractmeter (made in Netherlands, 2007), with Cu kα radiation- λ=0.15406 nm, 45 kV and 40 mA", is employed in this work. Optical microscopy and scanning electron microscopy (SEM) were used to observe the microstructure of the metal substrates, view the surface topography of the oxidized scales and also to investigate the microstructures of the cross-section of the oxidized pellets. The optical microscope utilized was of the type "Olympus BX41M-LED" and the scanning electron microscope employed was of the type "FEI Company, Quanta 250 FEG Analyzer (made in Netherlands)". X-ray energy dispersive analysis (EDAX) was employed to determine the oxygen, chromium and nickel elemental content at selected spots of the samples. The EDAX analyzer was of the type FEI Company, Quanta 250 FEG (made in Netherlands). Oxygen, chromium and nickel profiles along the cross-sections of the oxidized pellets were obtained by using line EDAX analysis.

For the microstructure examination of the cross-sectional of the oxidized pellets, every sample was vertically mounted in a mold, then ground in turn with silicon carbide abrasive papers with grit size ranging from 80 to 800 until almost one half of the sample was removed, and then the cross-sections were polished with 0.3 μm alumina paste.

3. Results and Discussion

The kinetics of the oxidation process was measured for the three pellets of each type to examine the reproducibility of the process. The dependence of average weight gain per unit area on time for the three pellets of each type is shown in Figure 1; the standard deviations are also illustrated as vertical bars in Figure 1.

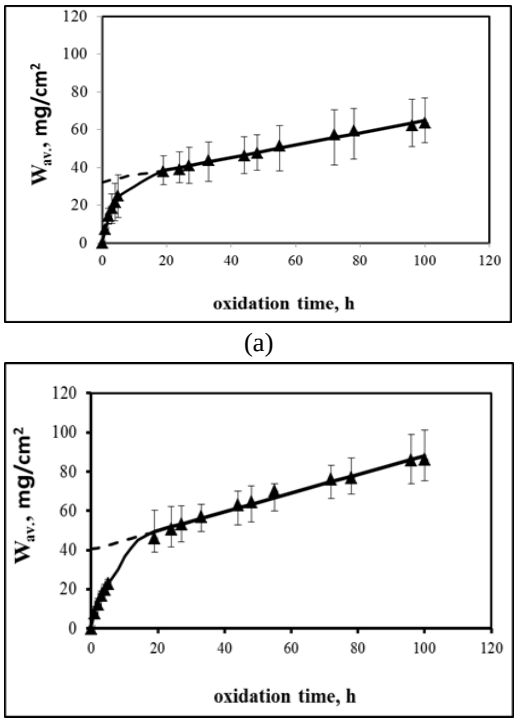

Fig. 1. The dependence of the average weight gain per unit area of three samples on oxidation time for the 4 wt% Cr pellets (a) and 8 wt% Cr pellets (b), the bars represent the standard deviation

The oxidation rate at different time is estimated by using the relation $\Delta W_{av}/\Delta t$, where ΔW_{av} is the change in the weight gain during the time period Δt. Figure 2(a) indicates that the oxidation rate of the 4 wt% Cr pellets is initially rapid, the black line in the figure, and then gradually decreases until it realizes a constant rate after 40 h where the linear rate constant value is about $8x10^{-8}$ (g/cm^2)/sec, the red line in the figure. Figure 2(b) reveals also that the oxidation rate for the 8 wt% Cr pellets is rapid at the initial stage, the black line in the figure then it decreases gradually until realizing a constant rate value of $20x10^{-8}$ (g/cm^2)/sec after about 72 h, , the red line in the figure. It is to be noticed that the steady oxidation rate for the 8 wt% Cr pellets was realized after longer time than that of the 4 wt% Cr pellets and the linear rate constant of the 8 wt% Cr is larger than that of the 4 wt% Cr alloy by about 2-3 times. This might be due to the higher thermal instability of the oxide scale formed on the 8 wt% Cr.

The value of the linear rate constant of porous-nickel at 1273K for 100 h was about $5.5x10^{-8}$ (g/cm^2)/sec [9]. For the same conditions, Ni-Cr alloys with 0.25, 0.5 and 1 wt% Cr have the average linear rate constants of the oxidation process were about $7.2x10^{-8}$, $8x10^{-8}$ and $5.7x10^{-8}$ (g/cm^2)/sec, respectively [10]. Increasing the Cr content to 12 wt% in the Ni-Cr alloy for the same conditions, decrease the linear rate from $1.9x10^{-8}$ to $6.9x10^{-8}$ (g/cm^2).sec with a great variation in the values due to the great irreproducibility [11].

Referring back to Figure 1, the figure shows that the oxidation rate is initially rapid for all pellets. However after some time of oxidation, very slow rate of oxidation was observed over several short time intervals, and then the initial values of oxidation rate were attained. This may be caused by the formation of protective parts of sublayers which fails again due to internal stresses. Figure 1 also shows a sudden increase of weight gain per unit area for a short period of time during the oxidation process and then it starts to slow down again nearly to the steady-state linear rate. This rapid increase might arise from the development of more easy migration paths in the oxide scale which allow more molecular oxygen migration [12, 13]. These easy paths for molecular oxygen migration might be due to the development of internal stresses within the oxide scales [12, 13].

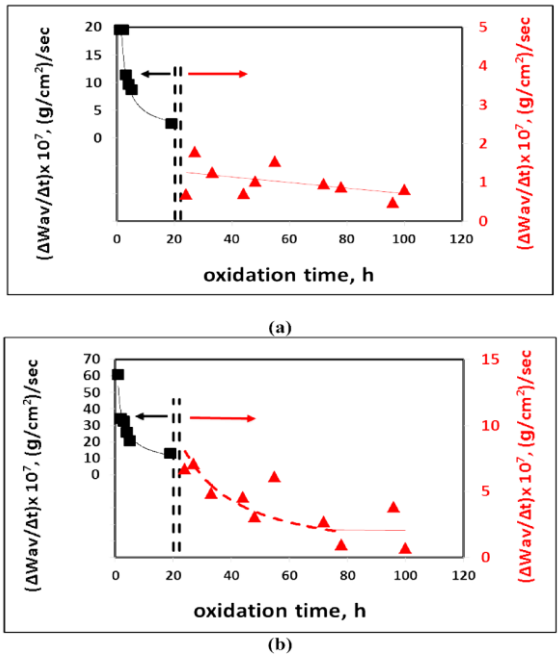

Fig. 2. The dependence of the slope of the curve of Fig. 1. representing the dependence of the average weight gain on oxidation time for the 4 wt% Cr pellets (a) and the 8 wt% Cr pellets (b)

Microstructure Observation, Elemental Distribution, and Phase Analysis

The Ni-4 wt% Cr Porous Pellets

Figure 3 is a typical scanning electron image for the upper surface of an oxidized Ni-4 wt% Cr pellet after a total oxidation time of 100 h. Figure 4(a) shows the optical image of the cross-section of an oxidized 4 wt% Cr pellet. Figure 4(b) shows the SEM image of the cross-section of an oxidized 4 wt% Cr pellet. The optical image of Figure 4(a) and the SEM image of Figure 4(b) clearly indicated the formation of porous scale on the metal substrate; the porous scale was duplex consisting of larger outer layer and smaller inner layer partially separated from each other by cavities. The formation of a duplex scale might be initiated by loss of adherence between the single layer and the metal substrate due to the buildup of internal stresses within the chemical compound scale giving the chance of formation of a second layer between the higher chemical compound layer and therefore the metal substrate. Cavities were also noticed between the oxide scale and the metal substrate. The ratio of the outer layer thickness to the inner layer thickness differed from one part to another.

Spot EDAX analysis was carried out at spots (1) and (2) which are shown at the upper surface of the oxidized sample of Figure 3 and the results of EDAX analysis at Table 2. The results of spot EDAX analysis of spots (3), (4) and (5) which are shown in Figure 4 are given in Figures 5(a), (b) and (c), respectively. Spot (3) was located near the middle of the oxide scale. Spot (4) was positioned very close to the scale/metal interface within the scale side. The position of spot (5) was on the metal substrate and the data of the results of EDAX analysis for spots (3), (4) and (5) are summarized in Table 2.

TABLE 2. Spot EDAX results of the 4 wt% Cr pellets

Element	Spot No. (Element% Indicator)				
	1	2	3	4	5
O	14.04	13.25	10.87	15.64	0.88
Cr	0.26	0.35	1.72	2.21	0.75
Ni	85.7	86.4	87.41	82.15	98.37

X-ray diffraction patterns obtained at different depths of the oxide scale are shown in Figure 6. Nickel oxide was the only phase detected on the upper surface of the oxidized pellet and at depth x =0.28 L as shown in Figure 6(a) and Figure 6(b), respectively. Ni, NiO, $NiCr_2O_4$ and Cr_2O_3 peaks were observed in the pattern taken at x =0.61L as observed in Figure 6(c). At the oxide/metal interface (x ≈ L) peaks of Ni and $NiCr_2O_4$ are detected as shown in Figure 6(d). These patterns indicated the formation of $NiCr_2O_4$ at x=0.61 L; the NiO peaks extended over the whole length of the oxide scale with formation of $NiCr_2O_4$ and Cr_2O_3 as particles precipitating within the NiO layer at the inner part of the scale. The formation of $NiCr_2O_4$ particles was also notices inside the pores of the metal matrix by the appearance of $NiCr_2O_4$ peaks at the pattern of Figure 6(d) which is taken near the scale/metal interface.

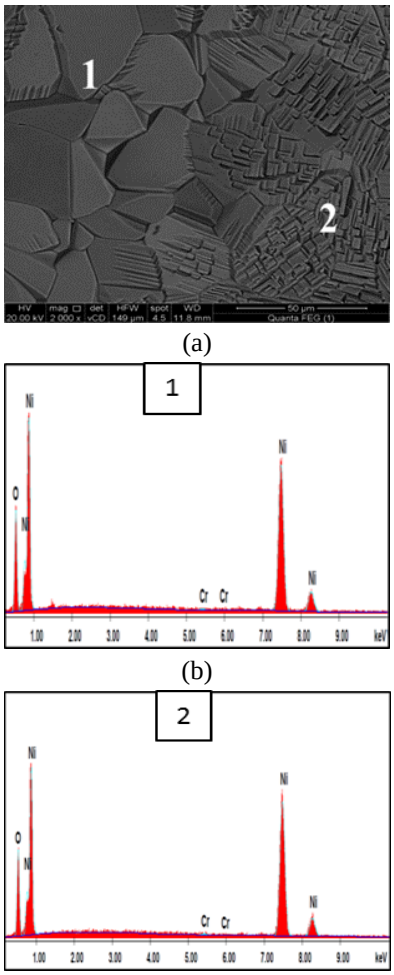

Fig. 3 (a) The SEM image of the upper surface of an oxidized Ni-4 wt% Cr pellet and the results of spot EDAX analysis at spots (1) and (2) on the upper surface

The XRD patterns obtained at different depth of the oxide scale agree with the results of spot EDAX analysis and the line profiles obtained for oxygen, chromium and nickel across the oxidized Ni-4 wt% Cr pellets. All of these results might be summarized in the following points: The oxygen and nickel profiles of Figure 5(b) indicate the formation of NiO duplex scale separated by cavities; the outer layer is much thicker than the inner layer. The results of spot EDAX analysis as well as the chromium and nickel profiles clearly

point out to the formation of extended NiO scale from the surface of the oxidized layer to the scale /metal interface with chromium solubility of about 0.26% in NiO at the outer surface of the oxide layer with gradual increase of chromium solubility in NiO along the cross-section of the scale. The nickel and chromium profiles of Figure 4(b) also indicate that the chromium-bearing oxides ($NiCr_2O_4$ and Cr_2O_3) particles are detected as precipices within the NiO matrix nearly at the inner half of the oxide scale while the particles were not observed at the outer part of the scale. In addition, $NiCr_2O_4$ particles were precipitated within the pores of the metal substrate.

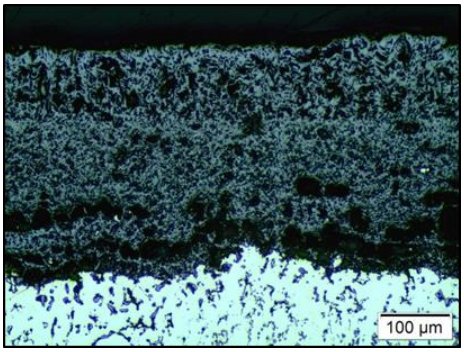

(a)

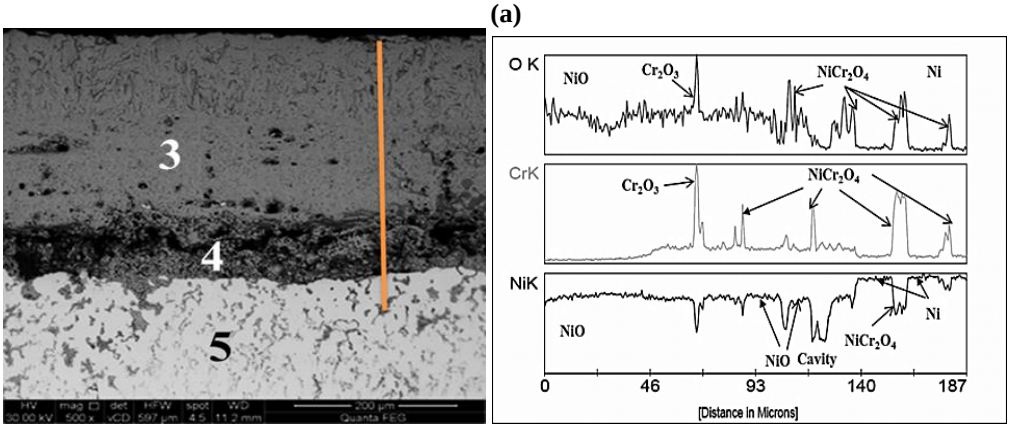

(b)

Fig. 4. (a) Optical image of the cross-section of an oxidized Ni-4 wt% Cr pellet and (b) SEM image of the cross-section of an oxidized Ni-4 wt% Cr after a total oxidation time of 100 h and the corresponding line EDAX profiles of O, Cr and Ni

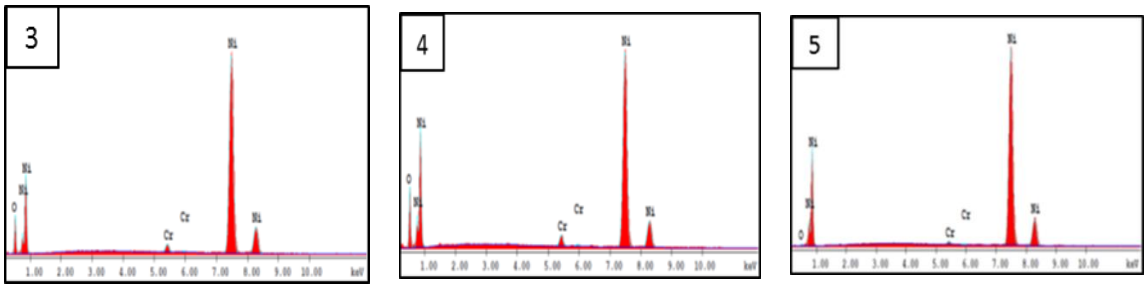

(a) (b) (c)

Fig. 5. Results of spot EDAX analysis for spot (3) (a), spot (4) (b) and spot (5) (c) on the cross-section of a Ni-4 wt% Cr pellet

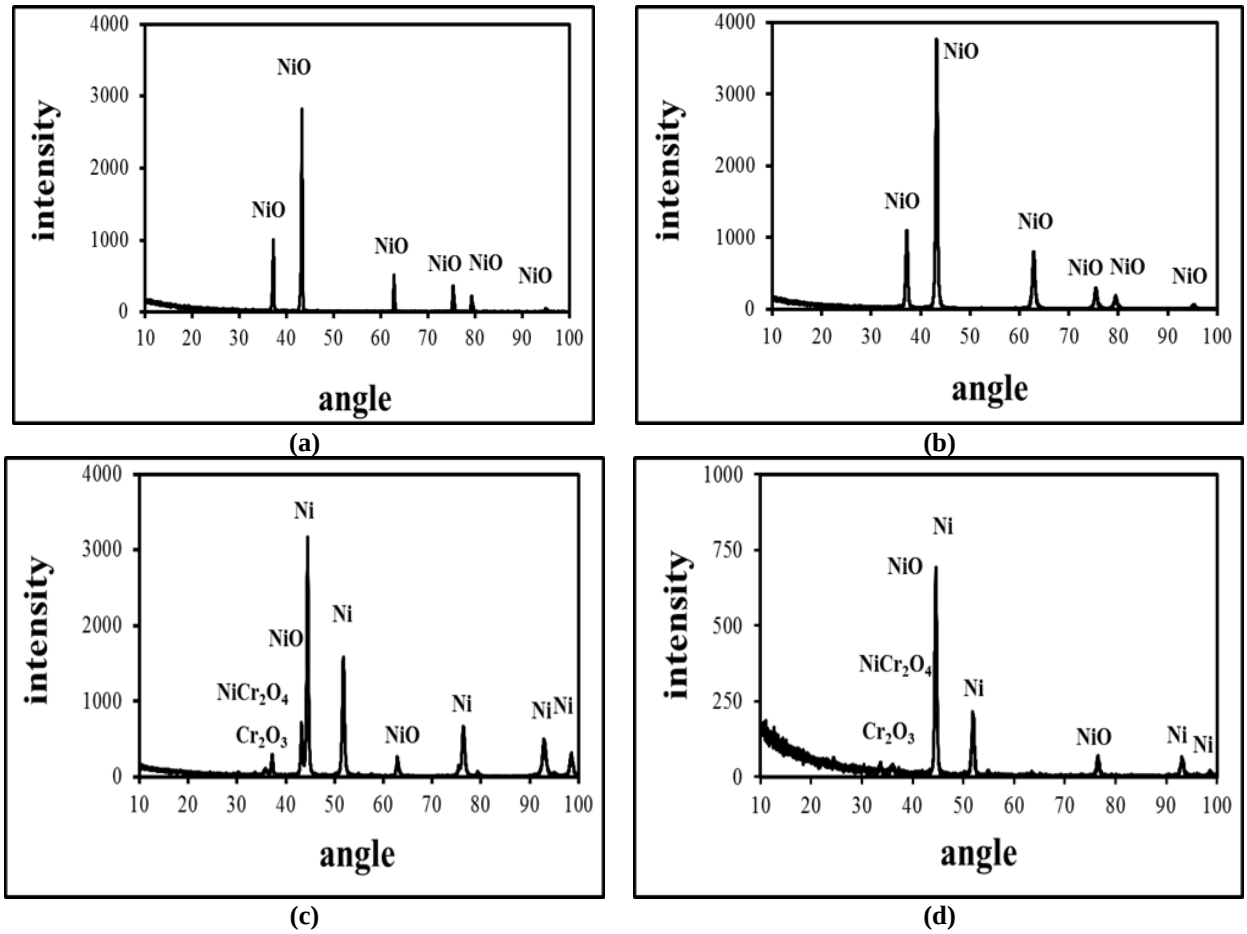

Fig. 6. X-ray diffraction patterns obtained for oxidized pellet of Ni-4 wt% Cr at the upper surface (x =0) (a), at x= 0.28 L (b), at x = 0.61 L (c) and near the metal/oxide interface (x≈L) (d)

The Ni-8 wt% Cr Porous Pellets

Figure 7 is a typical scanning electron image for the upper surface of an oxidized Ni-8 wt% Cr pellet after a total oxidation time of 100 h. The same figure shows spots (1) and (2) at which spot EDAX analysis is carried out. Transgranular cracks are formed at the upper surfaces of the oxidized samples as shown in Figure 8 which illustrates a typical crack of this alloy. Figure 9(a) shows the optical image of the cross-section of an oxidized 8 wt% Cr pellet; Figure 9(b) shows the SEM image of a typical cross-section of the oxidized 8 wt% Cr pellet. The optical image of Figure 9(a) and the SEM image of Figure 9(b) clearly indicate the formation of porous scale on the metal substrate. The oxide porous scale was formed from double layers consisting of outer layer which is partially separated from the inner layer by cavities.

The results of spot EDAX analysis at spot (1) and spot (2) are indicated in Table 3. Spot EDAX analysis was carried out on spots (3), (4) and (5) which are shown in Figure 9(b), the results obtained for spot (3), (4) and (5) are shown in Figures 10(a), (b) and (c), respectively. Spot (3) was located at the upper part of the oxide scale. The position of spot (4) was on a particle precipitated at the second layer. Spot (5) was located at the metal phase. The spot EDAX results for elemental percent are given in Table 3.

TABLE 3. Spot EDAX results of the 8 wt% Cr pellets

Element	Spot No. (Element% Indicator)				
	1	2	3	4	5
O	16.16	14.60	10.62	22.00	2.74
Cr	0.22	0.23	2.19	68.95	1.89
Ni	83.62	85.17	87.18	9.05	95.36

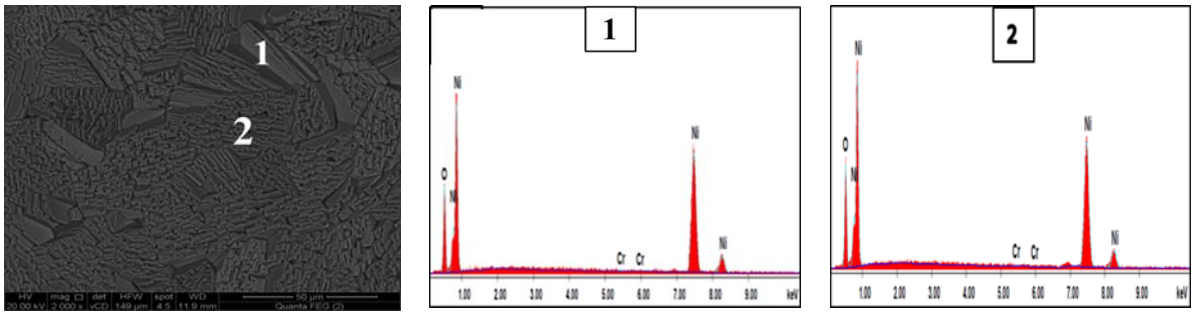

(a) **(b)** **(c)**

Fig. 7. The SEM image of the upper surface of an oxidized Ni-8 wt% Cr pellet and the results of spot EDAX analysis at spots (1) and (2) on the upper surface

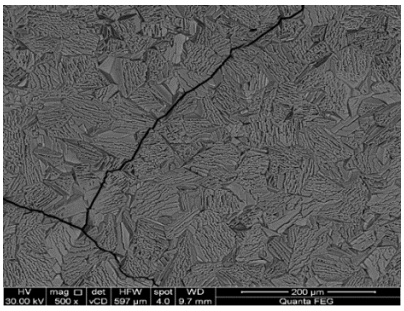

Fig. 8. The SEM image of the transgranular cracks of the Ni-8 wt% Cr sample

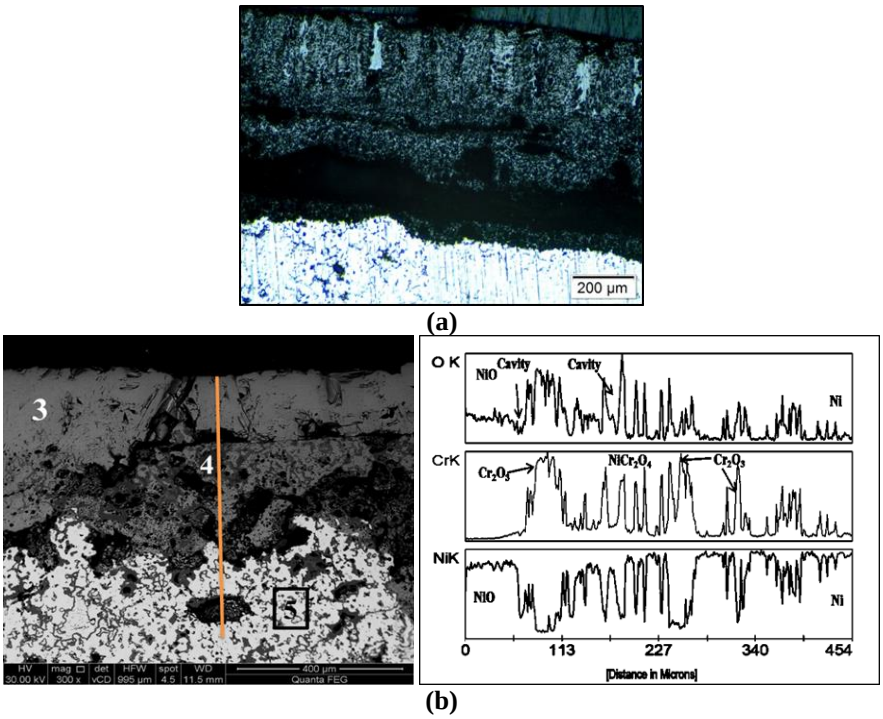

(a)

(b)

Fig. 9. (a) Optical image of the cross-section of an oxidized Ni-8 wt% Cr pellet and (b) SEM image of the cross-section of an oxidized Ni-8 wt% Cr after a total oxidation time of 100 h and the corresponding line EDAX profiles of O, Cr and Ni

X-ray diffraction patterns obtained at different depths of the oxide scale are shown in Figure 11. Nickel oxide was the only phase detected on the upper surface of the oxidized pellet as shown in Figure 11(a). Ni, NiO, $NiCr_2O_4$ and Cr_2O_3 peaks were observed in the pattern taken at x =0.4 L and at depth x =0.67 L as shown in Figure 11(b) and Figure 11(c), respectively. While Ni, NiO and Cr_2O_3 peaks were observed at the

oxide/metal interface (x ≈ L) as shown in Figure 11(d). These patterns indicated the appearance formation of $NiCr_2O_4$ at x=0.4 L; the NiO peaks extended over the whole length of the oxide scale with formation of $NiCr_2O_4$ and Cr_2O_3 as particles precipitating within the NiO layer.

The microstructure of the oxidized pellets, spot EDAX analysis for 5 spots (2 spots at the upper surface of an oxidized sample and 3 spots along its cross-section), oxygen, chromium and nickel profiles across the cross-section of the oxidized pellets, and X-ray diffraction patterns at the different depths of oxide scale reveled the following features: the oxide scale consisted of two layers, the upper layer is separated from the inner layer by cavities. The oxide scales as a whole was highly porous with formation of transgranular cracks. The outer layer of the oxide scale consisted of a single NiO phase with chromium solubility of about 0.22% at the upper surface of the scale which gradually increases with the depth of the oxide scale. The chromium solid solution in NiO phase extends through the outer layer and even through the inner layer. Spinel and Cr_2O_3 particles were precipitated at the inner layer. Nickel spinel particles were formed within the pores of the metal substrate.

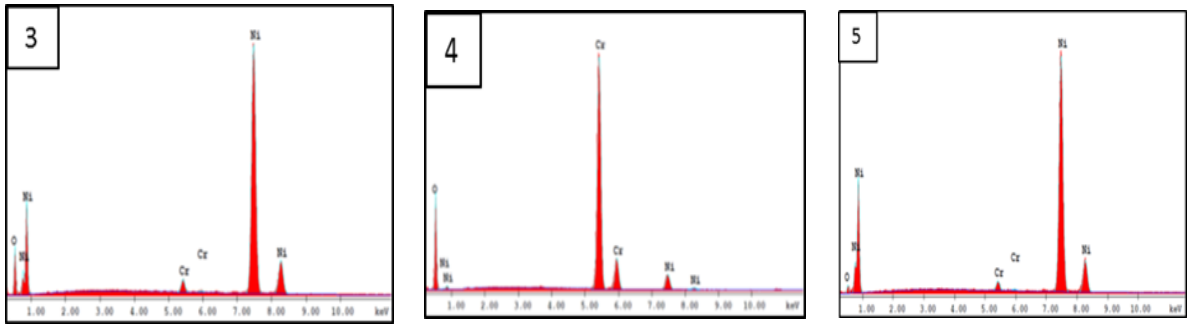

(a) (b) (c)

Fig. 10. Spot EDAX results of spot (3) (a), spot (4) (b) and spot (5) (c) of the cross-section of the Ni-8 wt% Cr pellet

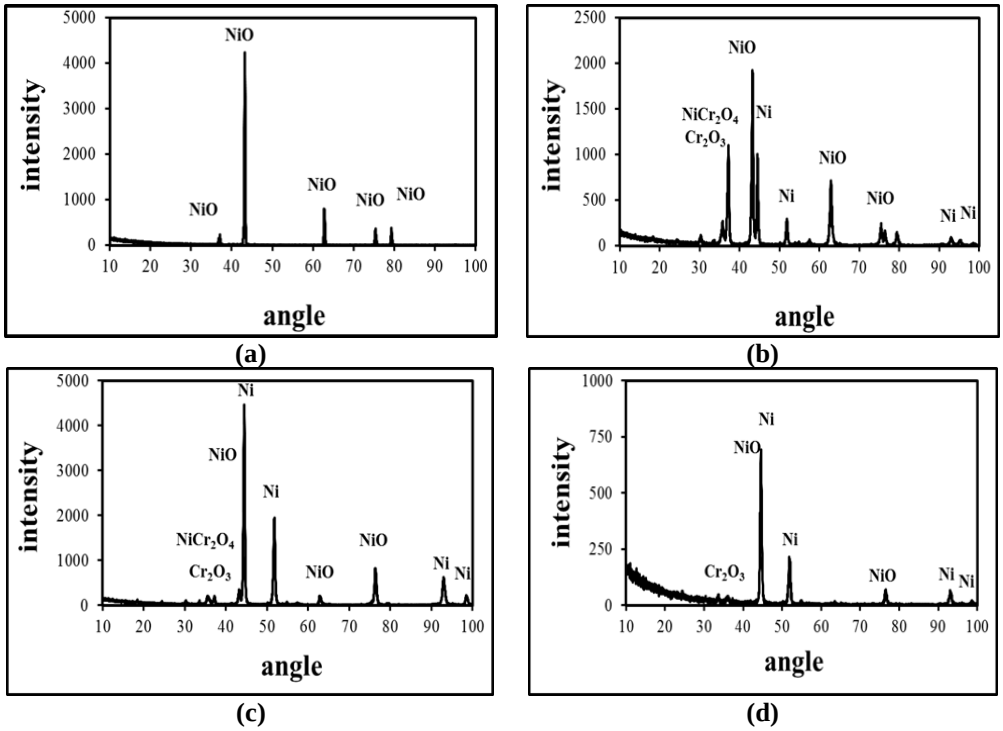

(a) (b) (c) (d)

Fig. 11. X-Ray diffraction patterns obtained for oxidized pellet of Ni-8 wt% Cr at the upper surface (*x* =0) (a), at *x*= 0.4 L (b), at *x* = 0.67 L (c) and near the metal/oxide interface (*x*≈L) (d)

Oxidation Mechanism

The characteristics of the formed oxide scales (porous oxide scales with cavity formation, transgranular cracks, and microfissures) indicated the growth of the scale by inward migration of molecular oxygen [12, 14, 15, 16] rather than by the outward cationic diffusion. The dependence of the average weight gain per unit area on time for both alloys the (4 wt% Cr and the 8 wt% Cr) indicated that the oxidation rate was initially rapid and then gradually decreased until realizing a constant rate. However, kinetic oxidation curves for individual samples (three for the 4 wt% Cr alloy and three for the 8 wt% Cr alloy) reflected the high thermal instability of the formed oxide scales. Each kinetic curve had several regions of discontinuity either due to slower rate of oxidation and/or rapid oxidation rate. This was in reflection to buildup of oxides sublayers that hinder the inward migration of molecular oxygen or formation of if new easy diffusion paths for inward oxygen migration through the scales, respectively. Because of the high affinity of chromium to oxygen and the inward migration of molecular oxygen, Cr-bearing oxides (Cr_2O_3 and $NiCr_2O_4$) might be formed at the scale/metal interface. Therefore, Cr-depletion at the metal/scale interface would occur; accordingly, the metal composition at the metal/oxide interface would be nearly pure nickel for the two types of alloys. This means that newly formed nickel oxide layers were added to the scale/metal interface at the scale/metal interface. Also spinel could be formed by the following reaction [14]:

$$NiO + Cr_2O_3 \rightarrow NiCr_2O_4 \quad (3)$$

Because nickel oxide is a metal deficient p-type oxide, the following substitutional dissolution doping reaction of Cr^{3+} in the cationic lattice of $Ni_{1-x}O$ might occur [17].

$$Cr_2O_3 \rightarrow 2\,Cr_{Ni}^{\cdot} + V_{Ni}^{\prime} + 3\,O_O^x \quad (4)$$

Also, the inward migration of molecular oxygen through the porous metal pellet precipitated chromium as $NiCr_2O_4$ internal particles in all examined alloys. The oxidation of the nickel base-metal into nickel oxide at the scale/metal interface would extend from the outer surface of the scale to the scale/metal interface. This interface would move to the inside of the metal phase because of the inward molecular oxygen migration. Thus, the internally precipitated Cr-bearing oxides particles get incorporated in the newly formed NiO layers which therefore were either dissolved completely in the nickel oxide layer or forming two phases region of nickel oxide and nickel spinel phases.

4. Conclusion

The oxidation behavior of porous 4 wt% Cr and 8 wt% Cr alloys in air at 1273K of 100 h is investigated. It is concluded as the following:

- The average growth rate of the weight gain of both alloys is initially rapid and then decreases gradually until realizing constant rate after about 40 h for the 4 wt% Cr alloys and after about 72 h for the 8 wt% Cr alloys.
- The linear rate constants for the 4 wt% Cr and the 8 wt% Cr alloys are $8x10^{-8}$ $(g/cm^2)/sec$ and $20x10^{-8}$ $(g/cm^2)/sec$, respectively.
- A duplex oxide scale is formed on both alloys. Cavities are noticed between the outer and the inner layers in both alloys and also between the inner layer and the metal substrate.
- Nickel-chromium spinel ($NiCr_2O_4$) and Cr_2O_3 fine particles are precipitated within the inner parts of NiO phase while the outer parts are free from both particles. Nickel-chromium spinel ($NiCr_2O_4$) particles are formed within the pores of the metal substrate.
- The oxidation process is based on the inward migration of molecular oxygen through the easy migration paths (pores, transgranular cracks and others) which exist within the scale and the metal substrate; accordingly, the newly formed layers of oxides are added to the oxide scale at the scale/metal interface.

5. Conflicts of interest

There are no conflicts to declare

6. References

1. Ameer M.A., Abdel Hamid Z., Shehata M., Hassan B.M., and Fekry A.M., The impact of cationic surfactants on the electrodeposition of nickel/graphene nano-sheet composite coatings on brass, Egypt. J. Chem. 62(2): 201 - 214 (2019)
2. Langli L., Lianfeng Z., Daniel K.S., Donald R.B., Stephen M.B., Guangwen Z., and Chong-Min W., In-situ transmission electron microscopy study of

surface oxidation for Ni–10Cr and Ni–20Cr alloys. Scripta Materialia. 114, 129–132 (2016)
3. Kumar M., Singh H., and Singh N., Fire side erosion–corrosion protection of boiler tubes by nanostructured coatings, Mater. Corro., 666(7): 695-709 (2014)
4. Gada H., Mudgal D., Parvez S., and Ahmad B., Investigation of high temperature corrosion resistance of Ni25Cr coated and bare 347H SS in actual husk fired boiler atmosphere, Eng. Failure Analysis, (2019)
5. Zima E.G., Some high temperature oxidation characteristics of nickel with chromium additions. Project Designation NR 031-355, California Institute of Technology, (1956)
6. Hauffe K., Oxidation of metals. 179 (1965)
7. Caplan D., Graham M.J., and Cohen M., Effect of cold work on the oxidation of nickel at high temperature. J Electrochem Soc: Solid-State Sci Technol. 119(9), 1205-1215 (1972)
8. Wood G.C., Hodgkiess T, and Whiitle DP. A comparison of the scaling behaviour of pure iron-chromium and nickel-chromium alloys in oxygen. Corr. Sci. 6, 129-147 (1966)
9. Mohamed L.Z., Ghanem W.A., El kady O.A., Lotfy M.M., Ahmed H.A., and Elrefaie F.A., Oxidation characteristics of porous-nickel prepared by powder metallurgy and cast-nickel at 1273K in air for total oxidation time of 100 h, J Adv. Research. (JAR), 8 , 717-729 (2017)
10. Mohamed L.Z., Ghanem W.A., El kady O.A., Lotfy M.M., Ahmed H.A., and Elrefaie F.A., Oxidation Characteristics of Porous Nickel Low-Chromium Binary Alloys in Air at 1273K for 100 h, Key Eng. Mater.(KEM) , 786, 37-43 (2018)
11. Mohamed L.Z., Ghanem W.A., El kady O.A., Lotfy M.M., Ahmed H.A., and Elrefaie F.A., Oxidation characteristics of porous Ni-12 wt%Cr alloy at 1000 °C in air, Ain Shams Eng. J, 9, 2993–3000 (2018)
12. Chevalier S., Desserrey F., and Larpin J.P., Oxygen transport during the high temperature oxidation of pure nickel. Oxid Met. 64(314), 219-234 (2005)
13. Przybilla, and Schutze M., Role of growth stresses on the structure of oxide scales on nickel at 800 and 900°C. Oxidation of Metals. 58(1/2), 103-145 (2002)
14. Atkinson H.V., A Review of the role of short-circuit diffusion in the oxidation of nickel, chromium, and nickel-chromium alloys. Oxidation of Metals. 24(3/4), 177-197 (1985)
15. Kofstad P., On the formation of porosity and microchannels in growing scales. Oxid Met. 24(5/6): 265-276 (1985)
16. Mrowec S., On the mechanism of high temperature oxidation of metals and alloys. Corr Sci. 7: 563-578 (1967)
17. Anton C., Oxidation-induced phase transformations and lifetime limits of chromia-forming nickel-base alloy 625. Master, (2011)